Experimental Study of the Spectral Distribution of the Light Scattered from Flexible Macromolecules in Very Dilute Solution

Chi Wu,*,† Kam Kwong Chan,† and Ke-Qing Xia‡

Departments of Chemistry and Physics, The Chinese University of Hong Kong, Shatin, N.T., Hong Kong

Received July 29, 1994; Revised Manuscript Received November 14, 1994®

ABSTRACT: Spectral distributions (SD) of the light scattered from three high molecular weight polystyrene standards in dilute solution over a wide range of scattering angles (5.7−154°) were precisely determined from a series of carefully executed light scattering experiments. At $x \ll 1$, the SD have only one narrow peak, where $x = (qR_g)^2$, with q being the scattering vector and R_g the radius of gyration of the polymer coil. As expected, this peak is purely due to translational diffusion and has a line width $\Gamma_{peak1} = Dq^2$, with D being the diffusion coefficient of polymer. In the intermediate range of $1 < x \leq 15$, the SD have two peaks. We have identified that the normalized line width $\Gamma_{peak2}/(Dq^2)$ of the second peak is associated with the internal motions and follows the plot of $[1 + 2\Gamma_n/(Dq^2)]$ versus x, wherein Γ_n is the line width associated to the nth-order internal motion with $n = 1$ in $1 < x < 3$; $n = 2$ in $3 < x < 6$; $n = 3$ in $6 < x < 10$; and $n = 4$ in $10 < x < 15$. Thus, we can obtain Γ_n from $\Gamma_{peak2}/(Dq^2) = [1 + 2\Gamma_n/(Dq^2)]$. These measured Γ_n values agree with the predicted values according to the non-free-draining bead-and-spring model. However, the same model also predicts that, for $3 < x < 15$, the contribution from $[1 + 2\Gamma_1/(Dq^2)]$ should be dominant in the SD. This contradiction between the theory and observation leads us to believe that some of the energy-favored internal motions are not observable in dynamic LLS at particular x, which is related to the observation length scale ($1/q$). For $x > 15$, the two peaks merge into one broad peak. The plot of $\langle\Gamma\rangle_z/(q^3k_BT/\eta_0)$ versus $x^{1/2}$ of this peak approached a plateau value which is lower than a theoretically predicted value, where $\langle\Gamma\rangle_z$, k_B, T, and η_0 are the z-average line width, the Boltzmann constant, the absolute temperature, and the solvent viscosity, respectively.

Introduction

As one of the fundamental problems in polymer physics, the dynamics of flexible polymer chains in dilute solution has been theoretically investigated and experimentally examined for a number of years.[1−6] It has been shown that the relaxation processes associated with internal motions of flexible polymer chains in dilute solution will add additional broadening to the spectral distribution of the scattered light.[7] Quantitative predictions on the degree of this spectral broadening have been made on the basis of the bead-and-spring dynamical models with or without considering hydrodynamic interactions.[8,9] But, these theories are not very successful in describing the measured spectral distributions at large values of $x = (qR_g)^2$, where R_g ($= \langle R_g^2\rangle_z^{1/2}$) is the root-mean-square z-average radius of gyration and $q = (4\pi n/\lambda_0)\sin(\theta/2)$ is the scattering vector, with n, λ_0, and θ being the solvent refractive index, the light wavelength in vacuo, and the scattering angle, respectively.

As stated in a recent publication,[10] the study of intramolecular relaxation processes in dilute solution remains a difficult experimental challenge. In order to observe as many internal modes as possible, a long flexible polymer chain, i.e., a high molecular weight sample, has to be used. For such a polymer, there always exists a certain degree of coupling between the translational diffusion and the internal motions at the lowest accessible scattering angle (~15°) of a normal laser light scattering (LLS) spectrometer. Without a clear separation of these two types of motions, it is impossible to have a good and reliable investigation of the spectral distribution of very long polymer chains in dilute solution. Recently, Chu *et al.*,[10] using a combination of a specially designed low-angle LLS spectrometer with a prism cell and a conventional wide-angle LLS spectrometer, have studied this complicated problem. By choosing an appropriate x range, they observed two internal relaxation times (τ_1 and τ_2), especially the τ_2 value of a flexible polymer coil in dilute solution for the first time. However, there was no explanation given as to why they observed the second internal mode instead of the first one, which was expected to be dominant in their x range according to the bead-and-spring model.

Partly motivated by this apparent contradiction between the theory and experimental observation, we carried out an experimental study reported here with our specially aligned LLS spectrometer equipped with a precise goniometer, which is capable of doing both static (absolute intensity measurement) and dynamic LLS experiments continuously from the scattering angle of 5.7° to 154°. To our knowledge, this wide and continuous scattering angle range has not been reported before.

First, we intended to confirm the internal motions observed by Chu *et al.* with a series of carefully designed and executed LLS experiments; second, if their results could be confirmed, our speculation was that we might be able to observe the higher order internal motions, such as τ_3, τ_4, and so on as x increases beyond the x range reported by them; third, if our speculation was right, we would have to reexamine the existing theoretical predictions and try to find out why there exists a discrepancy between the theories and experimental results.

Theoretical Background

As was shown by Pecora, when an infinitely dilute polymer solution is illuminated by a coherent and monochromatic laser light beam, the spectral distribution of the light scattered from a flexible polymer chain can be written as[11]

† Department of Chemistry.
‡ Department of Physics.
® Abstract published in *Advance ACS Abstracts,* January 15, 1995.

0024-9297/95/2228-1032$09.00/0

$$S(q,\omega) = (1/2\pi)\int e^{-i\omega t} e^{-q^2 D|t|} J(q,t)\, dt \qquad (1)$$

where ω is the difference between the angular frequency of the scattered light and that of the incident light, q is the scattering vector as previously defined, D is the translational diffusion coefficient for the center of mass of the polymer chain, and the function

$$J(q,t) = \langle (1/N^2) \sum_{l=0}^{N}\sum_{m=0}^{N} e^{-i\mathbf{q}[\mathbf{r}_l(0)-\mathbf{r}_m(t)]} \rangle \qquad (2)$$

is the spatial Fourier transform of the segment–segment time correlation function. It arises from the interference of the scattered lights from different segments in a polymer chain with N such segments. It contains all the temporal and spatial information on the intramolecular (or internal) motion of a polymer chain. Here $\mathbf{r}_l(0)$ is the position of the lth segment at time 0, and $\mathbf{r}_m(t)$ is that of the mth segment at time t; both are referred to the center of mass of the polymer.

In order to perform the ensemble average in $J(q,t)$, an explicit model for the internal motion of a chain is needed. By incorporating the Oseen–Kirkwood–Riseman hydrodynamic interaction into the bead-and-spring model, Perico, Piaggio, and Cuniberti (PPC) have shown[12]

$$S(q,\omega) = P_0(x)\, L(\omega,q^2D) + \sum_{\alpha=1}^{N} P_1(x,\alpha)\, L(\omega,q^2D+\Gamma_\alpha) + \sum_{\alpha=1}^{N}\sum_{\beta=1}^{N} P_2(x,\alpha,\beta)\, L(\omega,q^2D+\Gamma_\alpha+\Gamma_\beta) + \sum_{\alpha=1}^{N}\sum_{\beta=1}^{N}\sum_{\gamma=1}^{N} P_3(x,\alpha,\beta,\gamma)\, L(\omega,q^2D+\Gamma_\alpha+\Gamma_\beta+\Gamma_\gamma) + \ldots \qquad (3)$$

where the functions

$$L(\omega,\Gamma) = \frac{2\Gamma}{2\pi(\omega^2+\Gamma^2)} \qquad (4)$$

represent the ω-normalized Lorentzian distributions, with Γ being the half-width at half-height, i.e., the line width, and the P_ns (n = 0, 1, 2, ...) determine the contributions of the different Lorentzians to the spectrum of the scattered light. The zeroth-order $P_0(x)$ represents the contribution of the translational diffusion; $P_1(x,\alpha)$, the first-order contribution of the αth internal mode; $P_2(x,\alpha,\beta)$, the second-order contribution of the αth and βth internal modes; and so on. When $x < 1$, the spectral distribution is measured in the long-wavelength regime and hence $P_0(x)$ is dominant in $S(q,\omega)$. As x increases, the contributions from $P_1(x,\alpha)$, $P_2(x,\alpha,\beta)$, and other higher-order terms become more and more important. PPC have numerically shown that $P_2(x,1,1)$ is the largest contribution to $S(q,\omega)$ among all Lorentzian terms associated with the internal modes.[12]

In a modern dynamic laser light scattering experiment, the intensity–intensity time correlation function of the scattered light is usually measured from which $S(q,t)$, the Fourier transform of $S(q,\omega)$, is determined.

Experimental Section

Sample Preparation. Three high molecular weight and narrowly distributed polystyrene standards (Batch No. 20147-7, nominal $M_w = 6.50 \times 10^6$, $M_w/M_n = 1.06$; 20148-5, $M_w = 1.02 \times 10^7$, $M_w/M_n = 1.17$; and 20149-4, $M_w = 1.44 \times 10^7$, $M_w/M_n = 1.21$) from Polymer Laboratories Ltd., denoted hereafter as HPS-1, HPS-2, and HPS-3, and analytical grade toluene, from Riedel-deHaen Co. were used in this study. The polymer concentrations were very dilute (~30 μg/mL), so that the concentration correction on the measured line-width distribution was very small (<4% on the basis of the known value of the second-virial coefficient). In this concentration range and at high scattering angle, the scattering intensity was so weak that the signal-to-noise ratio could drop down from ~0.9 to as low as ~0.05. An overnight data accumulation therefore is required in order to have a good dynamic light scattering measurement. Thus, it is essential to prepare a clean solution, with all dust particles removed from the solution; otherwise, the light scattered from even one or two remaining dust particles will ruin the measured time correlation function.

We took the following precautions in our solution preparation: (1) prepare dust-free toluene with a 0.02 μm filter (ANOTOP, Whatman); (2) clean all needles, syringes, and even volume flasks with a large amount of dust-free solvent; and (3) prepare the solution in a dust-free volume flask with the dust-free toluene. By adopting these precautions, the only dust particles present in the solution were from polymer itself. Before the light scattering measurement, the solution was filtered once more with a 0.5 μm filter (Millipore) to insure the scattered intensity fluctuation per second at small angle is less than ±3% during the entire measurement.

Static Laser light Scattering (Static LLS). For a Gaussian coil in a dilute solution, the angular (θ) dependence of the absolute time-averaged scattered intensity over solvent, known as the excess Rayleigh ratio [$R_{vv}(\theta)$], can be expressed as[13,14]

$$\frac{KC}{R_{vv}(\theta)} \cong \frac{1}{M_w p(x)} + 2A_2C \qquad (5)$$

where $K = 4\pi^2 n^2 (dn/dC)^2/(N_A\lambda_0^4)$ and $p(x) = (2/x^2)(x - 1 + e^{-x})$, with N_A, dn/dC, n, and λ_0 being Avogadro's number, the specific refractive index increment, the solvent refractive index, and the wavelength of light in vacuo, respectively. Again, $x = (qR_g)^2$. A_2 is the second virial coefficient. Benoit has shown[15] that, for long polymer chains, the determination of $p(x)$ over a wide range of x gives not only the weight-average molecular weight M_w from the small x range but also the number-average molecular weight M_n and z-average molecular weights M_z in the asymptotic portion of $p(x)$ at $x \gg 1$. In addition, at $x < 1$, we can determine R_g from the plot of $1/p(x)$ versus q^2.

Dynamic LLS. An intensity–intensity time correlation function $G^{(2)}(t,\theta)$ in the self-beating mode is normally measured and has the following form:[16,17]

$$G^{(2)}(q,t) = A[1 + \beta|g^{(1)}(q,t)|^2] \qquad (6)$$

where A is a measured base line; β, a spatial coherence constant depending only on the detection optics, with its value ($0 \le \beta \le 1$) reflecting the signal-to-noise ratio of the actual experiment; and $g^{(1)}(q,t)$, the normalized electric field time correlation function. It can be shown that $g^{(1)}(q,t)$ is proportional to the dynamic structure factor $S(q,t)$ and $g^{(1)}(q,t)$ can be related to the line-width distribution $G(\Gamma)$ by[17]

$$g^{(1)}(q,t) = \int_0^\infty G(\Gamma)\, e^{-\Gamma t}\, d\Gamma \qquad (7)$$

A Laplace inversion of eq 7 gives $G(\Gamma)$. The inversion can be accomplished by using, for example, a CONTIN algorithm.[18] For a monodisperse hard-sphere sample, $G(\Gamma)$ is a delta function. But, for the flexible polymer chains, even for a truly monodisperse sample, $G(\Gamma)$ is a distribution with a finite width. This is because a flexible polymer coil has a conformation distribution in dilute solution. Different conformations have different diffusion coefficients which lead to a distribution in Γ. Thus, the width of $G(\Gamma)$ consists of two parts. One is from the sample polydispersity, and the other is from the conformation distribution. This conformation broadening in $G(\Gamma)$ has been overlooked in the past. For a narrowly distributed polymer sample, at $x \ll 1$, $G(\Gamma)$ is a translational diffusion

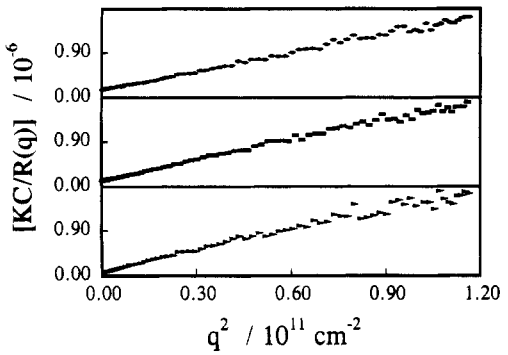

Figure 1. Typical plots of $KC/R(q)$ versus q^2 from static LLS experiments for HPS-1, HPS-2, and HPS-3, respectively from top to bottom, in toluene at 20 °C.

Table 1. Summary of Static and Dynamic LLS Results at $x < 1$[a]

sample	M_n ($\times 10^6$)	M_w ($\times 10^6$)	M_z ($\times 10^6$)	R_g (nm)	D ($\mu m^2/s$)	$(M_z/M_w)_{cal}$	$(M_w)_{cal}$ ($\times 10^6$)
HPS-1	6.10	6.33	6.78	130	4.43	1.08	6.09
HPS-2	9.80	10.4	13.4	210	3.25	1.12	10.4
HPS-3	16.4	19.8	24.4	311	2.25	1.20	19.7

[a] Relative errors are as follows: M_n, M_w, and M_z, ±2%; R_g, ±3%, D, ±1%.

coefficient distribution. When $x > 1$, the contributions from the internal relaxation processes to $G(\Gamma)$ become more and more appreciable.

LLS Instrumentation. A commercial LLS spectrometer (ALV/SP-150 equipped with an ALV-5000 multi-τ digital correlator) was used with a solid-state laser (ADLAS DPY525II, output power ≈ 400 mW at $\lambda = 532$ nm) as the light source. The incident beam was vertically polarized with respect to the scattering plane. In our setup, β in eq 6 was ~ 0.9, a rather high value for an LLS spectrometer capable of doing static and dynamic LLS simultaneously. Because of this high β value, we were able to carry out dynamic LLS in an extremely dilute solution with a reasonable signal-to-noise ratio. The solid laser beam had a nominal diameter of 0.32 mm which was ~5 times smaller than that of a normal Ar ion gas laser. We have modified the detection system by adding a pinhole as near the light-scattering cell as possible to reduce the angular uncertainty. With this laser and a proper alignment, we have made our present LLS spectrometer capable of doing both static and dynamic LLS continuously from the scattering angle of 5.7−154°. The precise dn/dC value at $T = 20$ °C and $\lambda = 532$ nm was determined by a novel differential refractometer which was designed and constructed in our laboratory.[19] All measurements were done at $T = 20.0 \pm 0.1$ °C. The details of LLS instrumentation and its principles can be found elsewhere.[16]

Results and Discussion

In the Range of $x < 1$. Figure 1 shows respectively from top to bottom three typical plots of $KC/R(q)$ versus q^2 from static LLS experiments for HPS-1, HPS-2, and HPS-3 in toluene at 20 °C. As stated in the last section, the extrapolation of $KC/R(q)$ versus q^2 in the range of $x < 1$ gives M_w and R_g from the intercept and slope, respectively. Figure 1 shows that the extrapolation to $q = 0$ is really not necessary since our accessible lowest scattering angle is already close to zero. On the other hand, the linear fitting of $KC/R(q)$ versus q^2 in the range of $x \gg 1$ gives us M_n and M_z.[15] Such obtained M_n, M_w, and M_z at finite concentration were extrapolated to $C = 0$ by using the known A_2 values[20] on the basis of eq 5. All fitted values of M_n, M_w, M_z, and R_g from the static LLS are summarized in Table 1, which shows that HPS-1 and HPS-2 are fairly monodisperse and HPS-3 has a slightly broader distribution. The R_g values in Table 1 were used later in calculating x for the analysis of dynamic LLS results.

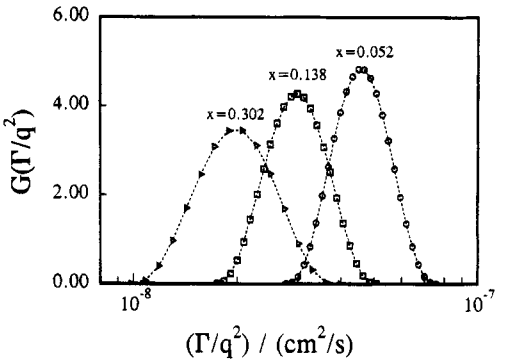

Figure 2. Typical line-width distributions $G(\Gamma/q^2)$ of HPS-1 (○), HPS-2 (□), and HPS-3 (△) in toluene at 20 °C and $\theta = 5.7°$ which respectively corresponds to $x = 0.052$, 0.138, and 0.302 for HPS-1, HPS-2, and HPS-3.

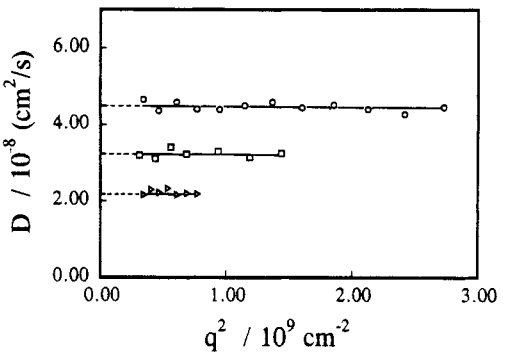

Figure 3. Plot of D ($=\langle\Gamma\rangle_z/q^2$) versus q^2 for HPS-1 (○), HPS-2 (□), and HPS-3 (△) where $\langle\Gamma\rangle_z = \int G(\Gamma)\,\Gamma\,d\Gamma$ and the highest scattering angles θ for HPS-1, HPS-2, and HPS-3 are 17° ($x = 0.450$), 12.3° ($x = 0.634$), and 9° ($x = 0.743$), respectively.

Figure 2 shows three typical line-width distributions $G(\Gamma/q^2)$ obtained from the CONTIN analysis of HPS-1 (○), HPS-2 (□), and HPS-3 (△) in toluene at $T = 20$ °C and $\theta = 5.7°$. This small scattering angle (5.7°) corresponded to $x = 0.052$, 0.138, and 0.302 for HPS-1, HPS-2, and HPS-3, respectively. The z-average line width $\langle\Gamma\rangle_z$ can be calculated from $G(\Gamma)$ ($\langle\Gamma\rangle_z = \int G(\Gamma)\,\Gamma\,d\Gamma$), and the variance μ_2 is defined as $\int G(\Gamma)\,(\Gamma - \langle\Gamma\rangle_z)^2\,d\Gamma$. The values of the relative width $\mu_2/\langle\Gamma\rangle_z^2$ of the distribution were very small (0.02−0.05) which further indicates that all polystyrene samples used in this study are narrowly distributed. In Table 1, the calculated polydispersity indexes $(M_z/M_w)_{cal}$ were estimated from the measured relative width $\mu_2/\langle\Gamma\rangle_z^2$ by using the relation[10] $(M_z/M_w)_{cal} \approx (1 + 4\mu_2/\langle\Gamma\rangle_z^2)$. Table 1 shows that $(M_w/M_n)_{cal}$ are close to the corresponding ratio of M_z and M_w from the static LLS.

Figure 3 shows a plot of D ($=\langle\Gamma\rangle_z/q^2$) versus q^2 in a regime of $x \ll 1$ for HPS-1 (○), HPS-2 (□), and HPS-3 (△). In this small x range, D seems to be independent of q^2. The contributions of the internal motions to the spectral distribution are insignificant, so that D approaches the z-average translational diffusion coefficient $\langle D\rangle_z$ when $x \to 0$. After extrapolating to infinite dilution, we obtained $\langle D\rangle_z(\theta=0,C=0)$ which is denoted as D hereafter. The measured values of D for HPS-1, HPS-2, and HPS-3 are listed in Table 1. Also listed were $(M_w)_{cal}$ obtained from the measured D by using a known scaling relation:[20] $D = 3.64 \times 10^{-4} M_w^{-0.577}$ for polystyrene in toluene at $T = 20$ °C. It can be seen that M_w from static LLS are very close to $(M_w)_{cal}$. We also calculated M_w (not listed) from R_g by using the scaling

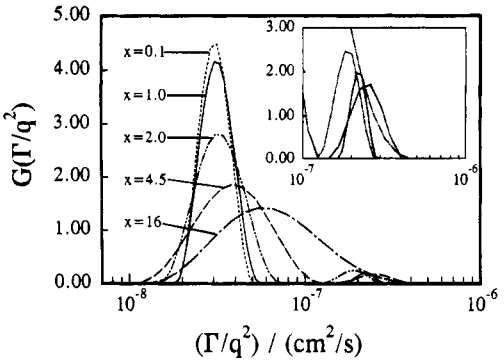

Figure 4. Typical plots of $G(\Gamma/q^2)$ versus Γ/q^2 for HPS-2 in toluene at 20 °C and different x values wherein the inset shows a ×10 enlargement of the second peak of the distribution in the range of 10^{-7}–10^{-6} cm^2/s.

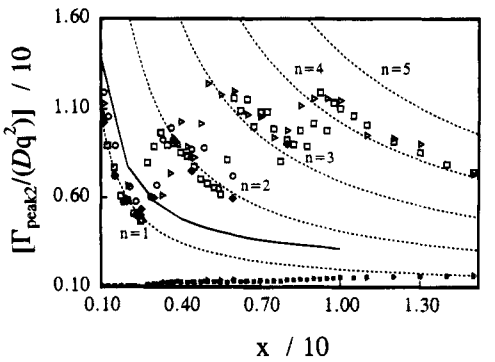

Figure 5. Plot of $\Gamma_{peak2}/(Dq^2)$ versus x for HPS-1 (○), HPS-2 (□), and HPS-3 (△) in toluene at 20 °C where Γ_{peak2} is denoted the average line width of the second peak (the larger symbols). For comparison, we included the average line width of the first peak (the smaller symbols). The filled diamonds and circles are the experimental results respectively from refs 10 and 21.

relation between R_g and M_w. The three M_w values from static and dynamic LLS are very close to each other. The good agreement among the M_w values from three different methods shows that the results reported in Table 1 are self-consistent and reliable, which indirectly shows that our LLS spectrometer was properly aligned and calibrated. Subsequently, the measured values of M_w (6.33×10^6, 1.04×10^7, and 1.98×10^7) were used in all analyses and calculations below.

In the Range of $x > 1$. Figure 4 show typical plots of $G(\Gamma/q^2)$ versus Γ/q^2 for HPS-2 in toluene at $T = 20$ °C and at different x values; the inset shows a ~10 enlargement of the second (smaller) peak of the distribution in the range of 10^{-7}–10^{-6} cm^2/s. We clearly see the following features in Figure 4. *First*, at $x < 1$, as expected and discussed above, there exists only one single and narrow peak. *Second*, at $x \sim 1$, a second peak with a higher Γ appears in $G(\Gamma/q^2)$, while the first peak is basically unchanged in position and shape. This second peak is related to the internal motions. *Third*, at higher x, the first peak is getting broader and shifting to higher Γ. This is because at higher x our LLS measurement scale (q^{-1}) is smaller than the chain dimension ($\sim R_g$), so that the contributions from the translational and internal motions are mixed in the measured spectrum which caused the broadening and shifting of the first peak. *Third*, at $x > 15$, the first and second peaks in $G(\Gamma/q^2)$ merge into a single and broader distribution. This can be explained by the fact that the line width (Dq^2) associated with the pure translational diffusion increases as x, but the line widths related to the internal motions are independent of the scattering angle.

Figure 5 shows a plot of $\Gamma_{peak2}/(Dq^2)$ versus x for HPS-1 (○), HPS-2 (□), and HPS-3 (△) in toluene at $T =$ 20 °C, where Γ_{peak2} is the average line width of the second peak (the larger symbols) in Figure 4. For comparison, the experimental data from Chu *et al.*[10] and Kurata *et al.*[21] (filled diamonds and filled circles, respectively) are also plotted in Figure 5. It can be seen that for comparable x values these data are in agreement with ours. In Figure 5, we also presented the normalized line width of the first peak $\Gamma_{peak1}/(Dq^2)$ smaller symbols). In the absence of any internal motions, its value should be 1. $\Gamma_{peak1}/(Dq^2)$ in Figure 5 is seen to increase slowly with x, and the plot of $\Gamma_{peak1}/(Dq^2)$ versus x is independent of M. This is due to (1) part of the internal motions with higher Γ are gradually mixed with the translational diffusion of the polymer chain and (2) the M-dependence of the diffusion part in the Γ_{peak1} has already been scaled by Dq^2. On the other hand, $\Gamma_{peak2}/(Dq^2)$ follows an unexpected pattern, and the plots of $\Gamma_{peak2}/(Dq^2)$ versus x for all three samples are independent of the molecular mass M. According to the existing theories for a flexible polymer coil in both the free-draining[22] and non-free-draining limits,[12] at $x > 1$, $S(q,t)$ depends mainly on the first five decay rates, namely, a pure translational term plus four principle intramolecular terms. In the decreasing order of contributions to the spectral distribution, eq 3 in the time domain at $x > 1$ can be written as

$$S(q,t) = P_0(x)\, e^{-Dq^2 t} + P_2(x,1,1)\, e^{-(Dq^2+2\Gamma_1)t} + P_1(x,2)\, e^{-(Dq^2+\Gamma_2)t} + P_4(x,1,1,1,1)\, e^{-(Dq^2+4\Gamma_1)t} + P_2(x,2,2)\, e^{-(Dq^2+2\Gamma_2)t} + \ldots \quad (8)$$

where the numeric values of P_n in the range of $1 \le x \le 10$ have been calculated by PPC.[12] On the basis of the Rouse–Zimm model,[2]

$$\Gamma_n = \frac{0.293RT\lambda_n'}{M[\eta]\eta_0} \quad (9)$$

where R, T, M, η_0, and $[\eta]$ are the gas constant, the absolute temperature, the polymer molecular mass, the solvent viscosity, and the intrinsic viscosity, respectively. λ_n' represents the eigenvalues in the Zimm model listed in ref 23. Using Dq^2 as a unit and replacing q with x, we can rewrite eq 9 as

$$\Gamma_n/(Dq^2) = \frac{0.293RT\lambda_n' R_g^2}{DM[\eta]\eta_0 x^2} \quad (10)$$

$\Gamma_n/(Dq^2)$ can be calculated from eq 10 with the known values of D, M, R_g, λ_n', η_0, and $[\eta]$ respectively in Table 1, in ref 23, and in the *Polymer Handbook*.[24]

Substituting the well-known scaling relations for a flexible polymer coil in good solvent[25,26] $R_g \propto M^{\alpha_R}$, $D \propto M^{-\alpha_D}$, and $[\eta] \propto M^{\alpha_\eta}$ with $\alpha_D \approx (1 + \alpha_\eta)/3$ and $\alpha_R \approx \alpha_D$ into eq 10, we can show that the plot of $\Gamma_n/(Dq^2)$ versus x should be independent of M for a given type of polymer, temperature, and solvent, which is exactly what we have observed in Figure 5.

By using the numeric values of P_n in ref 12 and the values of Γ_n calculated from eq 10, we are able to calculate the average line width $\langle\Gamma\rangle_{int}$ associated with the internal motions,[17] i.e.,

$$\langle\Gamma\rangle_{\text{int}} = [\sum_{\alpha=1}^{N} P_1(x,\alpha)\,(Dq^2 + \Gamma_\alpha) + \sum_{\alpha=1}^{N}\sum_{\beta=1}^{N} P_2(x,\alpha,\beta)\,(Dq^2 + \Gamma_\alpha + \Gamma_\beta) + \ldots]/[\sum_{\alpha=1}^{N} P_1(x,\alpha) + \sum_{\alpha=1}^{N}\sum_{\beta=1}^{N} P_2(x,\alpha,\beta) + \ldots] \quad (11)$$

According to PPC's theory, $\Gamma_{\text{peak}}/Dq^2$ calculated from the second peak of the line-width distribution in Figure 4 should follow the line of $\langle\Gamma\rangle_{\text{int}}/Dq^2$ versus x. However, the plot of $\langle\Gamma\rangle_{\text{int}}/Dq^2$ versus x (the solid line) in Figure 5 shows a clear deviation between the experimental data and the calculation.

On the basis of their calculation, PPC have predicted[12] that, in the range of $1 < x < 3$, only the second term in eq 8 gives a significant contribution to $S(q,t)$ and, at higher x, the higher terms together with the second term start to contribute to $S(q,t)$. In our experimentally accessible range of x, the second term is expected to be dominant. The dotted lines in Figure 5 represent plots of $[1 + 2\Gamma_n/(Dq^2)]$ versus x. It can be seen that the experimental data respectively follow the lines of $n = 1$ in $1 < x < 3$; $n = 2$ in $3 < x < 6$; $n = 3$ in $6 < x < 10$; and $n = 4$ in $10 < x < 15$. In other words, analyzing $\Gamma_{\text{peak2}}/(Dq^2)$ in Figure 4 by assuming that $\Gamma_{\text{peak2}}/(Dq^2) = [1 + 2\Gamma_n/(Dq^2)]$, we are able to determine Γ_1, Γ_2, Γ_3, and Γ_4 in different ranges of x. For $x > 15$, the two peaks in Figure 4 merge into one, which makes it difficult for us to get a precise Γ_{peak2} value from the spectral distribution. So, we stop our second-peak analysis of these high x value data in order to avoid any ambiguity.

Both Chu's and our experimental data clearly indicate that the internal motions associated with $2\Gamma_n$, i.e., $\Gamma_n + \Gamma_n$, dominate the relaxation process in different ranges of x, where n is the order of the internal motion. On the basis of eqs 3 and 8, this relaxation process is a self-coupling of the nth-order motion. At present, we have no explanation about why only this self-coupling internal motion was observed in dynamic LLS experiment. Energetically, it is easier to excite the internal motions associated with Γ_1 and $4\Gamma_1$ than that associated with $2\Gamma_2$. The fact that we observed $2\Gamma_2$ instead of Γ_1 and $4\Gamma_1$ in the range of $3 < x < 6$ might suggest that dynamic LLS's ability to measure certain internal modes is somehow related to the observation length scale, i.e., $1/q$. In other words, even though there exist some internal motions which are much more favorable from an energetic point of view, we could not "see" them in dynamic LLS in a certain range of x. If our speculation is right, the $P_n(x)$ values in ref 12 have to be modified to take into account the nature of dynamic LLS.

In the Range of $x > 15$. Figure 6 shows a plot of the reduced z-average line width $\Gamma/(q^3k_BT/\eta_0)$ versus $x^{1/2}$ for HPS-1 (○), HPS-2 (□), and HPS-3 (△) in toluene at 20 °C, where k_B is the Boltzmann constant. As x increases, the reduced z-average line width gradually decreases and approaches a plateau. This scaling of Γ with q^3 is consistent with the non-free-draining bead-and-spring model for flexible polymer chains in infinite dilute solution,[27] which was also observed by other laboratories in the past.[5,10,21] In general, the observed plateau values[10,21] (0.05−0.06) were significantly lower than the theoretical prediction (0.071 with preaveraged Oseen tensor and 0.079 without a preaveraged Oseen tensor[5]). In Figure 6, the plateau value of $\Gamma/(q^3k_BT/\eta_0)$ is around 0.05. This consistent lower plateau value shows that, at larger x, there exist some problems in the theoretically predicted $G(\Gamma)$.

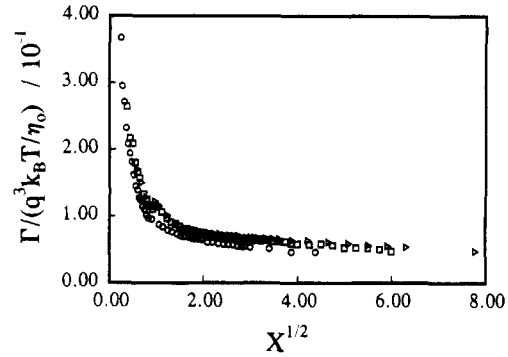

Figure 6. Plot of the reduced line width $\Gamma/(q^3k_BT/\eta_0)$ versus $x^{1/2}$ for HPS-1 (○), HPS-2 (□), and HPS-3 (△) in toluene at 20 °C, where T is the absolute temperature, and k_B, the Boltzmann constant.

In the above discussion, we have speculated that some of the energy-favorable internal motions cannot be observed in dynamic LLS experiment. If this were true, we might be able to explain the above lower plateau value as follows: On the basis of eq 3, we know that the terms associated with the internal motions have larger line widths than that of the pure translational diffusion of the center of mass (Dq^2). If some of the internal motions are not contributing as expected to the measured spectrum in dynamic LLS experiment, the z-average line width calculated from the line-width distribution will be smaller than that predicted in the bead-and-spring model for flexible coils. This smaller z-average line width will in turn lead to a lower plateau value. Further study is certainly needed to verify this speculation.

Conclusions

Our dynamic laser light-scattering results have shown that, for $x(qR_g)^2 > 1$, there are two peaks in the spectral distribution. The average line width Γ_{peak2} of the second peak associated with the internal motions does not follow theoretical predictions but a plot of $[1 + 2\Gamma_n/(Dq^2)]$ versus x, where $n = 1$ for $1 < x < 3$; $n = 2$ for $3 < x < 6$; $n = 3$ for $6 < x < 10$; and $n = 4$ for $10 < x < 15$. Our speculation is that some of the internal motions, though favorable in terms of energy, are not observable in a dynamic LLS experiment at particular x. This might be related to the observation length scale ($1/q$). The lower plateau value in the plot of $\Gamma/(q^3k_BT/\eta_0)$ versus $x^{1/2}$ may also be due to the same reason.

Acknowledgment. The partial financial support of this work by the RGC (the Research Grants Council of Hong Kong Government) Earmarked Grant 1994/95 (CUHK 299/94P, 221600260) is gratefully acknowledged.

References and Notes

(1) Rouse, P. E., Jr. *J. Chem. Phys.* **1953**, *21*, 1272.
(2) Zimm, B. H. *J. Chem. Phys.* **1956**, *24*, 269.
(3) Pecora, R. *J. Chem. Phys.* **1968**, *49*, 1032.
(4) de Gennes, P.-G. *Physics* **1967**, *3*, 37.
(5) Han, C. C.; Akcasu, A. Z. *Macromolecules* **1981**, *14*, 1080.
(6) Chu, B. *J. Polym. Sci., Polym. Symp.* **1985**, *73*, 137.
(7) Kramer, O.; Frederick, J. E. *Macromolecules* **1972**, *5*, 69.
(8) Fujimi, S.; Maruyana, M. *Macromolecules* **1973**, *6*, 237.

(9) Tagami, Y.; Pecora, R. *J. Chem. Phys.* **1969**, *51*, 3293.
(10) Chu, B.; Wang, Z.; Xu, J. *Macromolecules* **1991**, *24*, 6832.
(11) Pecora, R. *J. Chem. Phys.* **1965**, *43*, 1762.
(12) Perico, A.; Piaggio, P.; Cuniberti, C. *J. Chem. Phys.* **1975**, *62 (7)*, 2690; **1975**, *62 (12)*, 4911.
(13) Zimm, B. H. *J. Chem. Phys.* **1948**, *16*, 1099.
(14) Debye, P. *J. Phys. Colloid Chem.* **1947**, *51*, 18.
(15) Benoit, H. *J. Polym. Sci.* **1953**, *11 (5)*, 507.
(16) Chu, B. *Laser Light Scattering*; Academic Press: New York, 1974.
(17) Berne, B.; Pecora, R. *Dynamic Light Scattering*; Plenum Press: New York, 1976.
(18) Provencher, S. W. *Biophys. J.* **1976**, *16*, 29; *J. Chem. Phys.* **1976**, *64*, 2772; *Makromol. Chem.* **1979**, *180*, 201.
(19) Wu, C.; Xia, K.-Q. *Rev. Sci. Instrum.* **1993**, *65*, 587.
(20) Appelt, B.; Meyerhoff, G. *Macromolecules* **1980**, *13*, 657.
(21) Nemoto, N.; Makita, Y.; Tsunashima, Y.; Kurata, M. *Macromolecules* **1984**, *17*, 425.
(22) Sorlie, S. S.; Pecora, R. *Macromolecules* **1988**, *21*, 1437.
(23) Zimm, B. H.; Roe, G. M. *J. Chem. Phys.* **1956**, *24*, 279.
(24) Brandrup, J.; Immergut, E. H. *Polymer Handbook*, 3rd ed.; John Wiley & Sons: New York, 1989.
(25) de Gennes, P.-G. *Scaling Concepts in Polymer Physics*; Cornell University Press: Ithaca, NY, 1979.
(26) Flory, P. J. *Principles of Polymer Chemistry*; Cornell University Press: Ithaca, NY, 1953.
(27) Dubois-Violette, E.; de Gennes, P.-G. *Macromolecules* **1967**, *3*, 181.

MA9411686